Vernier microcombs for integrated optical atomic clocks

Downloaded from: https://research.chalmers.se, 2025-03-31 16:58 UTC

Citation for the original published paper (version of record):
Wu, K., O'Malley, N., Fatema, S. et al (2025). Vernier microcombs for integrated optical atomic clocks. Nature Photonics. http://dx.doi.org/10.1038/s41566-025-01617-0

N.B. When citing this work, cite the original published paper.

research.chalmers.se offers the possibility of retrieving research publications produced at Chalmers University of Technology. It covers all kind of research output: articles, dissertations, conference papers, reports etc. since 2004. research.chalmers.se is administrated and maintained by Chalmers Library

(article starts on next page)

nature photonics

Article

https://doi.org/10.1038/s41566-025-01617-0

Vernier microcombs for integrated optical atomic clocks

Received: 16 August 2023

Accepted: 8 January 2025

Published online: 19 February 2025

Check for updates

Kaiyi Wu[1,6] ✉, Nathan P. O'Malley[1,6], Saleha Fatema[1], Cong Wang[1,4], Marcello Girardi[2], Mohammed S. Alshaykh[3], Zhichao Ye[2], Daniel E. Leaird[1,5], Minghao Qi[1], Victor Torres-Company[2] & Andrew M. Weiner[1]

Kerr microcombs have drawn substantial interest as mass-manufacturable, compact alternatives to bulk frequency combs. This could enable the deployment of many comb-reliant applications previously confined to laboratories. Particularly enticing is the prospect of microcombs performing optical frequency division in compact optical atomic clocks. Unfortunately, it is difficult to meet the self-referencing requirement of microcombs in these systems owing to the approximately terahertz repetition rates typically required for octave-spanning comb generation. In addition, it is challenging to spectrally engineer a microcomb system to align a comb mode with an atomic clock transition with a sufficient signal-to-noise ratio. Here we adopt a Vernier dual-microcomb scheme for optical frequency division of a stabilized ultranarrow-linewidth continuous-wave laser at 871 nm to an ~235 MHz output frequency. This scheme enables shifting an ultrahigh-frequency (~100 GHz) carrier-envelope offset beat down to frequencies where detection is possible and simultaneously placing a comb line close to the 871 nm laser—tuned so that, if frequency doubled, it would fall close to the clock transition in $^{171}Yb^{+}$. Our dual-comb system can potentially combine with an integrated ion trap towards future chip-scale optical atomic clocks.

By virtue of their extreme long-term frequency stability, optical atomic clocks promise to revolutionize timing systems, enable fundamental tests of physics[1,2] and allow chronometric levelling and geodesy[2–4]. Bulky optical lattice clocks[2,4–6] and ion trap clocks[6,7] can provide state-of-the-art frequency stability. However, scaling these clocks to a low size, weight and power architecture is an important and challenging hurdle preventing ubiquitous deployment of the highest-performing optical atomic clock technology. Efforts such as refs. 8,9 towards integrated ion traps and optical lattices illustrate recent progress towards high-stability, chip-scale optical atomic clocks.

Microcombs are an essential part of future chip-scale optical atomic clocks[10,11] as they establish a coherent link from atomic references at hundreds of terahertz all the way down to the radio frequency (RF) domain (analogous to a gear set; Fig. 1a)[12] while preserving the stability of an atom-referenced clock laser. The realization of this coherent link is referred to as optical frequency division (OFD). The comb's optical modes f_m (m is the mode order) are equally spaced by the repetition rate f_{rep} (usually at RF), and the whole comb has a spectral offset (the carrier-envelope offset (CEO) frequency, f_{CEO}) so that $f_m = mf_{rep} + f_{CEO}$. Historically, frequency combs in optical atomic clocks have often been generated by mode-locked lasers[13–15] that have volumes on the order of

[1]School of Electrical and Computer Engineering, Purdue University, West Lafayette, IN, USA. [2]Department of Microtechnology and Nanoscience, Chalmers University of Technology, Gothenburg, Sweden. [3]Department of Electrical Engineering, College of Engineering, King Saud University, Riyadh, Saudi Arabia. [4]Present address: Department of Surgery, University of Pittsburgh, Pittsburgh, PA, USA. [5]Present address: Torch Technologies, Shalimar, FL, USA. [6]These authors contributed equally: Kaiyi Wu, Nathan P. O'Malley. ✉e-mail: wu1871@purdue.edu

https://doi.org/10.1038/s41566-025-01617-0

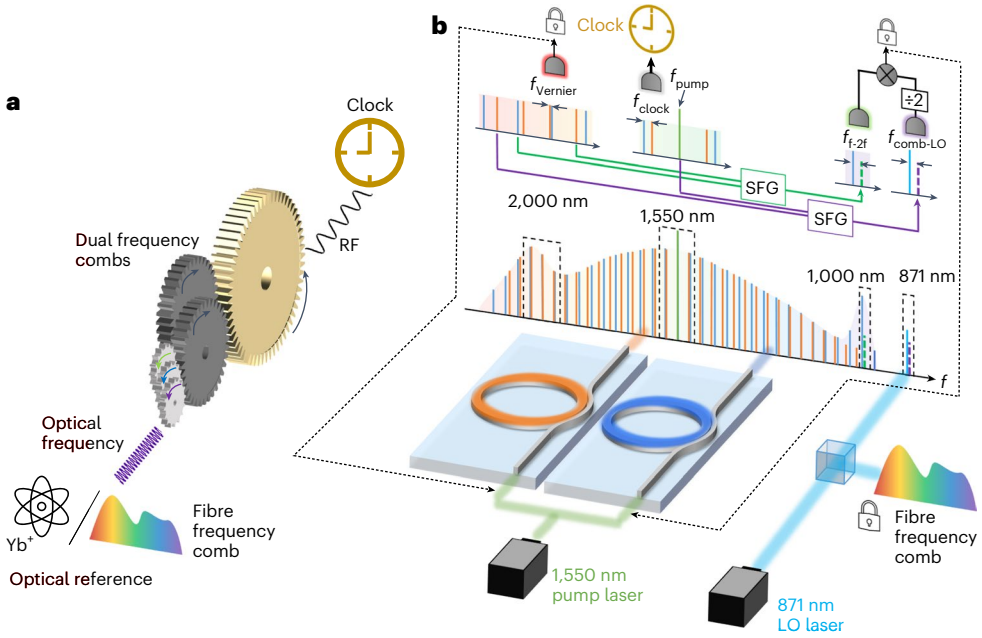

Fig. 1 | Overview of Vernier dual-microcomb scheme for OFD. a, An optical frequency comb system is analogous to a gear set, transferring the stability from optical frequency to RF. The large (small) size gears represent radio (optical) frequencies. The Vernier dual comb can further downconvert the RF by beating against each other. The optical reference can be a Yb^+ ion trap (as our system is designed for) or a stabilized FC (as a stable frequency proxy we adopted). **b**, An illustration of a Vernier dual-microcomb system for OFD. The dual combs excited by a shared pump at 1,550 nm generate broadband spectra spanning from ~1 μm to ~2 μm. The dashed boxes indicate the four spectral regions being used, and the zoom-in views are shown above. The first sidebands around the pump (near 1550nm) are used for RF clock output. The ~2 μm light is used for Vernier beat detection and the SFG process (green arrow line) for f-2f. The dual comb is related to the 871 nm LO laser through summing the pump and one of the Vernier comb lines at ~2 μm (purple arrow line), and the 871 nm laser is locked to a stabilized frequency comb. The dotted black lines indicate the feedback of the two locks to the pump intensities of the two combs.

many litres and generally require at least a measure of hand assembly, complicating mass production and increasing costs. Shrinking down these combs utilizing Kerr microresonators on photonic chips will be helpful towards miniaturizing optical atomic clocks and other systems requiring stabilized combs[16].

Unfortunately, Kerr microcombs possessing the octave span needed for self-referencing typically have ~1 THz repetition rates. This leads to f_{CEO} in the range of ±500 GHz, which is difficult to design because of microresonator fabrication imperfections[17,18]; hence, the f_{CEO} beat is frequently too high for electronic detection. Similarly, targeting a particular clock transition frequency through microresonator design and fabrication is challenging. Terahertz microcombs with their coarsely spaced lines have low chances of hitting the targeted frequency. In part due to these issues, microcomb-based OFD remains a challenging task. Although there are recent demonstrations on chip-based two-point OFD using a narrowband microcomb[19,20], such architecture is not applicable for single-point OFD from a single laser with f-2f self-referencing—a requirement for an optical atomic clock. The only two demonstrations[10,11] of microcomb-based OFD of atom-referenced lasers, to our knowledge, relied on low repetition rate (tens of gigahertz) and narrowband combs generated from millimetre-size silica disk resonators, either spectrally broadened in a nonlinear fibre[10] or paired with a secondary broadband silicon nitride (SiN) terahertz repetition rate microcomb[11]. Both of these works utilized thermal vapours for their atomic references with limited frequency stabilities compared with cooled or trapped atoms[8,9].

In this work, we demonstrate an integrated photonic platform based on Vernier dual-microcomb that overcomes some of the fundamental challenges of previous microcomb-based systems to realize chip-scale optical clocks. Specifically, by pairing a main octave-spanning terahertz repetition rate microcomb with a secondary broadband terahertz repetition rate Vernier microcomb, both on a SiN platform, we successfully frequency divide a continuous-wave laser at 871 nm (ref. 21) to an RF clock output at ~235 MHz. This laser is designed for frequency doubling to reach the ytterbium ion ($^{171}Yb^+$) clock transition at 435.5 nm, which supports better frequency stability[22] than thermal atomic references. By virtue of its dual broadband combs, the Vernier scheme used here presents substantial advantages over single broadband comb schemes. One of the advantages is the freedom of picking comb lines from either or both of the combs for sum-frequency generation (SFG) to aid in reaching a much greater variety of wavelengths[23]. Here, this is adopted both to help circumvent the high-frequency f_{CEO} detection problem and to reach 871 nm. Although our focus is on this transition, the technique is broadly applicable to other atomic transitions for future optical clocks. For example, SFG between the high-power pump and a comb line can cover ~600 nm to ~870 nm, which is viable for Ca^+ (729.1 nm) and Sr^+ (674.0 nm) clock transitions. In addition, with both terahertz microcombs fabricated in SiN films of the same thickness, there is potential to integrate our scheme on a single chip. Since the repetition rate of a microcomb scales as inverse of the microring circumference, the footprint of a dual ~1 THz microcomb structure could be several orders of magnitude smaller than architectures using ~20 GHz microcombs, enabling a higher manufacturing yield in mass production. Furthermore, the all-planar geometry used here avoids the complexity of coupling to suspended whispering gallery mode resonators or integrating them[24]. These results demonstrate a versatile and general microcomb platform to realize chip-scale optical atomic clocks.

Results

Dual-microcomb scheme

The overview of our experiment configuration is visualized in Fig. 1b. An ultranarrow-linewidth 871 nm (~344 THz) local oscillator (LO) laser developed by OEwaves[21,25] is phase-locked to an external

https://doi.org/10.1038/s41566-025-01617-0

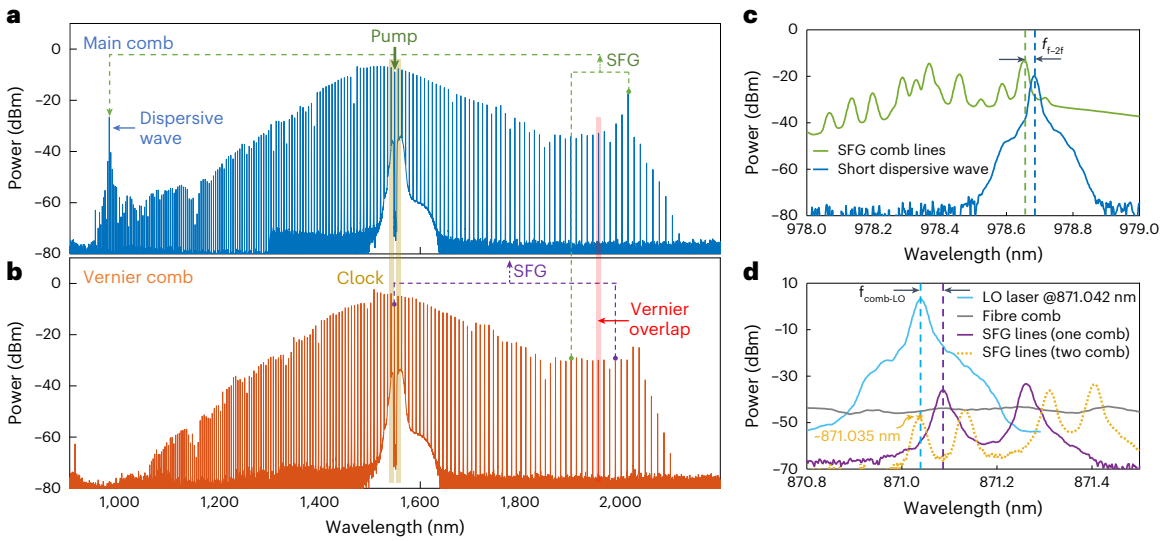

Fig. 2 | Optical spectra. a,**b**, The main comb (**a**) and the Vernier comb (**b**), each measured after pump suppression using a coarse wavelength-division multiplexing filter. **c**, The short-wavelength main comb line (dispersive wave) (blue) and the SFG lines at 1 µm (green) for f-2f beat detection. **d**, The 871 nm LO laser (light blue), the FC lines (grey) and the SFG lines at 871 nm (purple and yellow) generated by summing two lines from the same comb (purple) and by summing two lines from different combs (yellow). Detailed operation conditions for obtaining these two SFG curves can be found in Supplementary Section 5.2. The FC lines are spaced by ~250 MHz, which is smaller than the resolution of the optical spectrum analyser (~1 GHz). Hence, individual comb lines are not resolved here, and the trace appears featureless. The other spectra are comb-line resolved. **c** and **d** are measured at 0.01 nm resolution.

self-referenced fibre comb (FC), which serves as a frequency-stable proxy for a potential Yb^+ frequency reference (which is not available in our laboratory). The Vernier dual-microcomb scheme[23,26] is leveraged here for full OFD for the first time. Two broadband microcombs with large repetition rates (~900 GHz), slightly offset from one another ($\delta f_{rep} \approx 20$ GHz), are generated with a shared continuous-wave pump. This configuration has been shown to allow the detection of both large f_{rep} and f_{CEO} (ref. 23). We aim to transfer the LO laser stability to an RF clock output using a heterodyne beat in the dual-microcomb system.

We utilize a pair of microrings[27] (~25 µm radius) to generate microcombs. The main comb is designed to have dispersive waves at ~1 µm and ~2 µm wavelengths to assist the f-2f process, whereas the Vernier comb should have a resonance wavelength close to that of the main comb to allow a shared pump. Based on these criteria, we select microrings fabricated on separate chips but the same wafer. A single ~1,550 nm laser is amplified and split to pump both the main and Vernier devices simultaneously, generating an octave-spanning soliton microcomb in each. Figure 2a,b shows the spectra for the main and Vernier combs. The main (Vernier) comb possesses a repetition rate $f_{rep1} \approx 896$ GHz ($f_{rep2} \approx 876$ GHz). The pump frequency f_{pump} is ~193.54 THz, which can be written as $f_{pump} = f_{CEO1} + 216 f_{rep1} = f_{CEO2} + 220 f_{rep2}$. When the first sidebands from each comb are heterodyned together on a photodetector (Fig. 1b), they create an electronic signal oscillating at

$$f_{clock} = f_{rep1} - f_{rep2} \approx 19.7\ \text{GHz}. \quad (1)$$

Through appropriate feedback to our two combs, we seek to transfer the stability of the 344 THz LO laser to this ~19.7 GHz dual-comb beat.

To accomplish OFD from the LO laser to f_{clock}, at a minimum, we need to stabilize the two repetition rates to the LO laser. We separate the 1 µm, 1.55 µm and 2 µm spectral components and combine the dual-comb spectra at 1.55 µm and 2 µm wavelengths for the detection of various heterodyne beats. The spectral domain schematic is illustrated in Fig. 1b (the detailed experimental setup is described in Methods). Due to their different repetition rates, the two combs walk off from each other as one moves away from the pump frequency, eventually coming back together at the so-called Vernier overlap point. The comb modes at this point can be photodetected (here, around 1,945 nm) to produce a relatively low-frequency beat

$$f_{Vernier} = 44 f_{rep1} - 45 f_{rep2} \approx -8\ \text{GHz}. \quad (2)$$

With this signal phase-locked through feedback to the Vernier comb, f_{rep2} will follow f_{rep1} (ref. 28). We still need to stabilize the two repetition rates to the LO laser through feedback to the main comb to achieve a fully stabilized f_{clock} (equation (1)).

We perform a novel f-2f process via SFG[23] in a periodically poled lithium niobate (PPLN) waveguide, which sums one comb line from each comb at around 2 µm ($f_{CEO1} + 166 f_{rep1}$ and $f_{CEO2} + 179 f_{rep2}$). The sum products are combined with the short-wavelength side of the main comb around 1 µm ($f_{CEO1} + 342 f_{rep1}$) to create an f-2f-like beat, $f_{f\text{-}2f}$. Figure 2c shows the sample spectra of the sum products and the short wavelength line. This $f_{f\text{-}2f}$ contains contributions from both the f_{CEO} and the repetition rates of the combs

$$f_{f\text{-}2f} = f_{CEO2} - 176 f_{rep1} + 179 f_{rep2} \approx 11\ \text{GHz}. \quad (3)$$

Finally, to relate the dual microcombs to the LO laser, which is outside the span of both comb spectra, we use a second PPLN waveguide for SFG between the 1,550 nm pump ($f_{CEO2} + 220 f_{rep2}$) and a long-wavelength Vernier comb line ($f_{CEO2} + 171 f_{rep2} \approx 1{,}990$ nm) to create a nonlinear product. For OFD architecture demonstration, the LO laser is tuned to ~871.042 nm (a few gigahertz away from twice the Yb^+ clock transition wavelength of 871.035 nm) to beat against the SFG product to create $f_{comb\text{-}LO}$

$$f_{comb\text{-}LO} = 2 f_{CEO2} + 391 f_{rep2} - f_{871} \approx -19\ \text{GHz}. \quad (4)$$

Figure 2d shows the sample spectra for the SFG lines and the LO laser. This SFG process benefits from the high power of the pump and the optically amplified 2 µm comb line, leading to a reasonable SFG power of ~−36 dBm. We note that the Vernier scheme provides extra candidate

https://doi.org/10.1038/s41566-025-01617-0

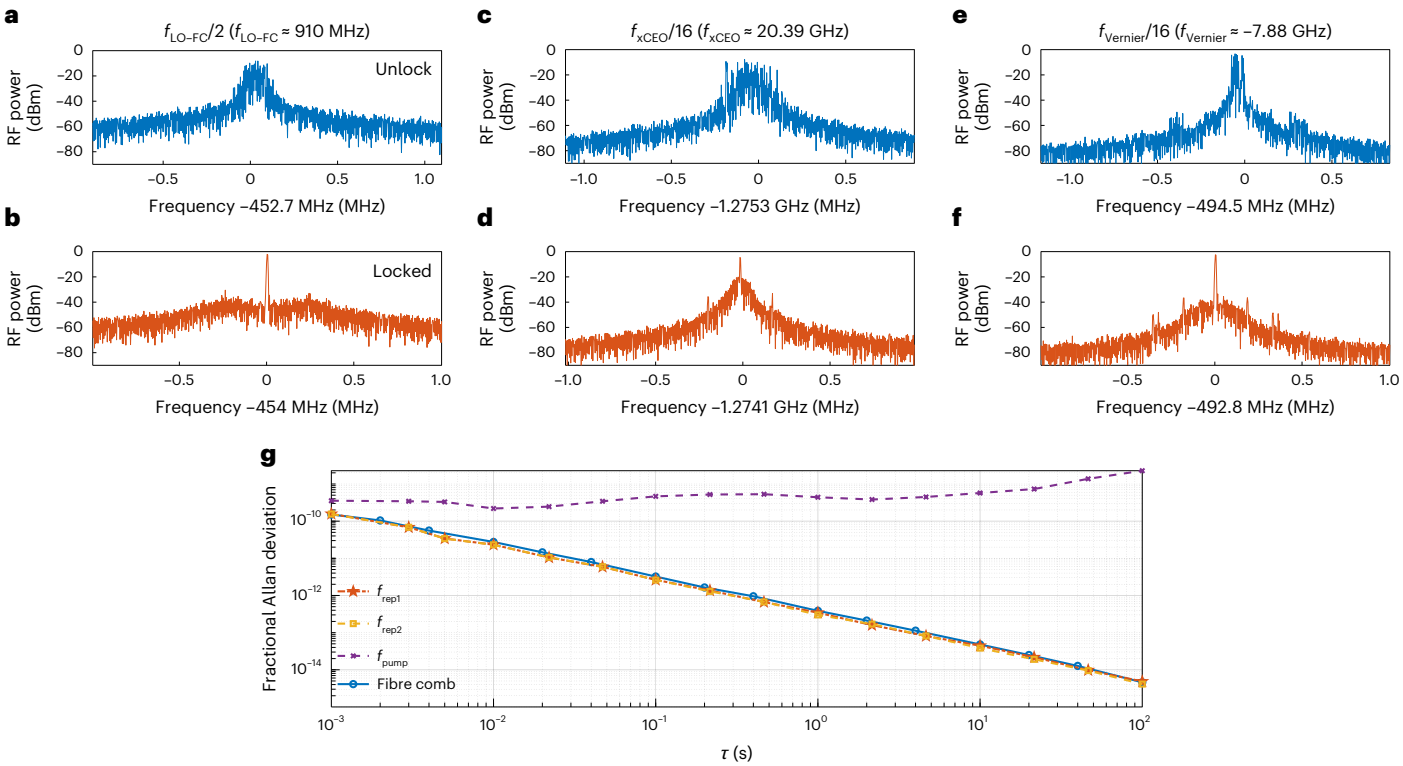

Fig. 3 | Microcomb stabilization. a–**f**, Electrical spectrum analyser traces of the three beats for stabilization: f_{LO-FC} (**a** and **b**), $f_{xCEO}/8$ (**c** and **d**) and $f_{Vernier}/8$ (**e** and **f**) when they are unlocked (blue traces) and phase-locked (orange traces). These traces are measured at the lockbox monitor outputs, and the beats are divided by an additional factor of 2. The resolution bandwidth is 3 kHz, and the spectral span is 2 MHz. **g**, The fractional Allan deviation of the repetition rates of the main (orange) and the Vernier (yellow) combs, the pump laser (purple) and the FC reference's repetition rate (and, hence, an estimate of its fractional optical stability) (blue).

lines in the SFG process by summing comb lines from different combs, where an SFG line right around 871.035 nm can be obtained (Fig. 2d and Supplementary Section 5.2).

As both $f_{f\text{-}2f}$ and $f_{comb\text{-}LO}$ contain the f_{CEO2} term, but with a fixed ratio of 1:2, we can cancel the CEO term through electronic frequency division and frequency mixing

$$\begin{aligned} f_{xCEO} &= f_{f\text{-}2f} - \frac{f_{comb\text{-}LO}}{2} \\ &= \frac{f_{871}}{2} - 176 f_{rep1} - 16.5 f_{rep2}. \end{aligned} \tag{5}$$

We refer to the frequency of the resulting signal as f_{xCEO} because, ideally, contributions from both combs' f_{CEO} are removed. Instead, f_{xCEO} depends on the two combs' repetition rates and relates them to the LO laser. If we lock this signal through feedback to the main comb and simultaneously lock $f_{Vernier}$ by feedback to the Vernier comb, the repetition rates will each be stabilized to the LO laser. As a consequence, f_{clock} should be stabilized, completing the clock frequency division. Importantly, this is irrespective of the free-running CEO frequencies of both combs. This simplifying scheme allows us to construct our clock system with two servos, removing requirements for a third servo to stabilize the offset frequency. The idea of eliminating a certain frequency comb instability to simplify a complex system is somewhat similar to the transfer oscillator concept for comparing two frequency standards[29].

Microcomb stabilization

To achieve the clock frequency division from the optical reference, we first stabilize the 871 nm LO laser to one optical line from a stable FC f_{FC} through an offset phase lock referenced to an RF synthesizer, where the offset frequency $f_{LO\text{-}FC} \approx \pm 910$ MHz (the sign is variable in our system) is defined as

$$f_{LO\text{-}FC} = f_{871} - f_{FC}. \tag{6}$$

We then phase-lock the f_{xCEO} and $f_{Vernier}$ beats to two other RF synthesizers by feedback to the pump power of the main and Vernier combs, respectively, using intensity modulators before input coupling to the two microrings. This stabilization scheme without CEO frequency locking avoids tuning the pump frequency and intensity simultaneously, which may introduce crosstalk between repetition rate and CEO frequency control[30]. Figure 3a–f shows the electrical spectrum analyser traces of the three beats before and after phase locking. The three RF synthesizers for the offset locks, the FC and the frequency stability testing utilities are all synchronized to a common GPS-disciplined oscillator (GPSDO) to eliminate relative drifting.

To verify the repetition rates for both microcombs are stabilized to the optical reference (i.e., FC), we conduct out-of-loop measurements using an electro-optic frequency comb[31] to downshift the repetition rates to an electronically detectable range. The time traces of the repetition rates are recorded by a zero dead-time frequency counter running at 1 ms gate time. We calculate the fractional Allan deviation of the two repetition rates, as shown in Fig. 3g. The frequency stability of the FC relative to the GPSDO is also obtained by measuring its ~250-MHz-repetition-rate beat note using a phase noise test set (PNTS) (Fig. 3g, blue trace). This is an estimate of the fractional frequency instability of the optical modes of the FC (Supplementary Section 2).

Both microcomb repetition rates follow the optical reference (Fig. 3g, orange and yellow traces), indicating that the stability of the LO laser has been successfully transferred to the two terahertz

https://doi.org/10.1038/s41566-025-01617-0

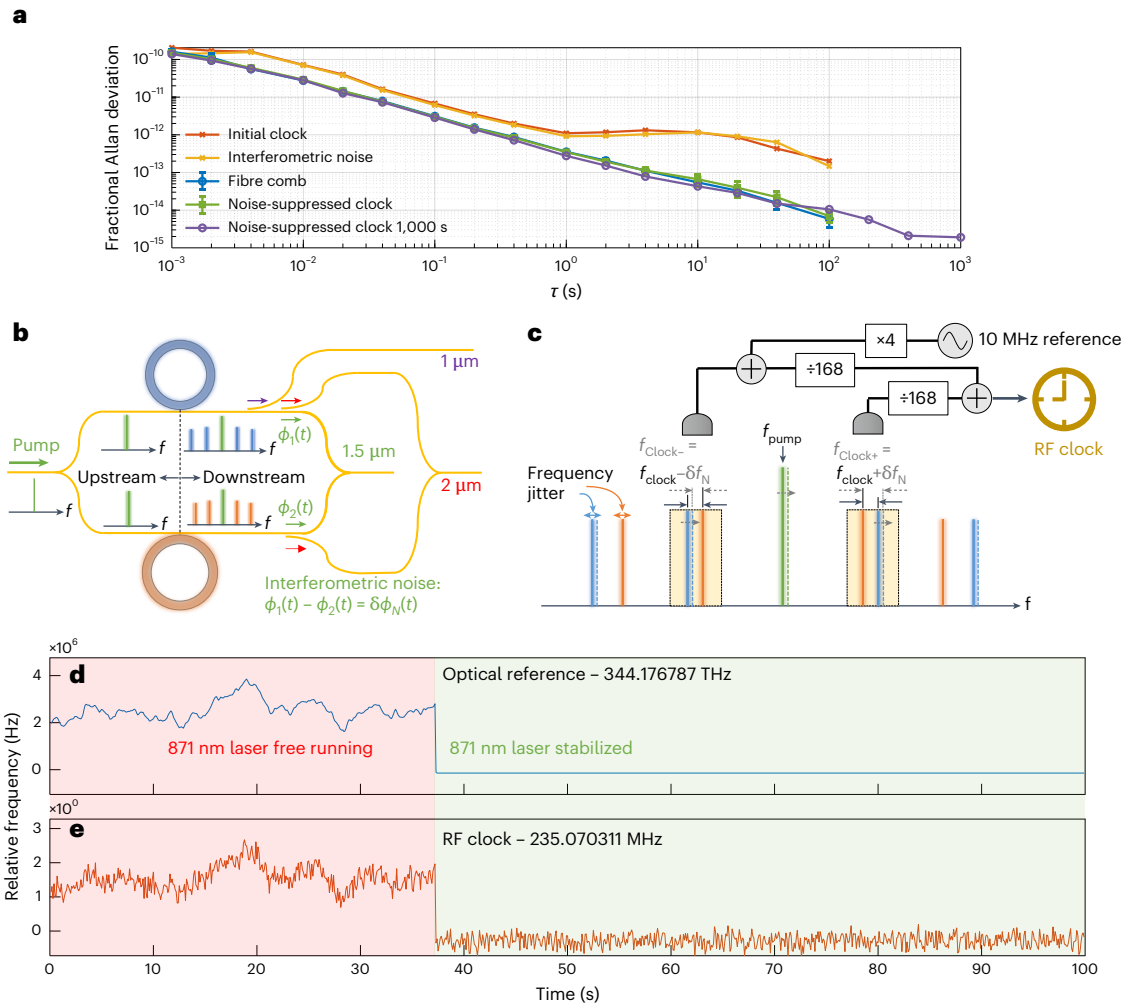

Fig. 4 | RF clock performance. a, The fractional Allan deviation of the clock without (orange) and with (green and purple) noise suppression, the extracted interferometric noise (yellow) and the optical reference (blue). **b**, Simplified dual-comb setup portraying the interferometric noise of this configuration. The blurring of the different comb lines represents frequency jitter due to interferometric phase noise. **c**, The noise suppression scheme exploiting dual clock signals (the dashed yellow boxes indicate the two optical filters to select them) generated using distinct photodetectors driven by main-Vernier comb line pairs at frequencies higher and lower than the pump frequency. The dashed comb lines illustrate a hypothetical case when the pump to the main ring (green line) and the resulting main ring comb lines (blue) are shifted up in frequency by time-varying phase $\phi_1(t)$, while the pump to Vernier ring and resulting Vernier comb lines are unaffected ($\phi_2(t) = 0$). The frequency noise of the RF beats generated from the higher and lower comb line pairs is strongly correlated but of opposite signs. Therefore, by summing the two clock signals with an electronic mixer, the interferometric frequency noise is largely suppressed. **d**,**e**, Frequency counter traces of the 871 nm laser (**d**) and the RF clock (**e**) with noise suppression. The 871 nm laser is initially free-running, then is locked at around 40 s. The f_{xCEO} and $f_{Vernier}$ locks are on throughout the measurement. The *y*-axis spans of the optical reference and the RF clock differ by their scaling factor of 17,292 × 84. The stabilized clock output exhibits a mean frequency of 235,070,310.72 Hz with a standard deviation of 0.18 Hz, limited by the counter measurement.

repetition rates while the combs' CEO frequencies remain free-running. We demonstrate this by beating the pump with a FC line at ~1,550 nm and recording the unstable output with a frequency counter (Fig. 3g, purple trace). Frequency division from f_{871} to f_{clock} is complete, following the expression (see further discussion in Supplementary Section 1)

$$f_{clock} = \frac{1}{17{,}292}\left(f_{871} - 2f_{xCEO} + 385f_{Vernier}\right) \approx \frac{1}{17{,}292} f_{871}. \quad (7)$$

RF clock performance

We characterized the fractional frequency instability of the RF clock output with the PNTS. The results are shown in Fig. 4a. Although, initially, the fractional instability (orange line, 'initial clock') decreases approximately inversely with the averaging time τ, as expected, it shows excess noise with ~5× higher fractional instability than our system floor (blue line, FC) and plateaus at a value of ~10^{-12} for $\tau \approx 1$ s and beyond. A similar effect has been reported in other recent works[32,33] but was not investigated therein. We attribute this excess noise to time-varying phase perturbations in the fibre leads that bring light in and out of the individual microrings, as illustrated in Fig. 4b. Related noise effects are well known in the distribution of ultrastable frequency references and coherent optical carriers over fibre links and are usually addressed by feedback control to an acousto-optic frequency shifter to stabilize a heterodyne beat involving two-way propagation through both the acousto-optic and the fibre link[34–36]. Here, we adopt an open-loop electronic mixing technique that reduces the excess noise from our clock signal without the need for two-way propagation and brings the frequency instability down to a level near our system floor, explained below. The idea is similar to the transfer oscillator scheme to remove residual fibre noise[37].

Because f_{clock} can be generated by photodetecting the first sidebands at either side of the pump (f_{clock+} and f_{clock-}), which carry frequency noise with equal amplitude but opposite sign, we can suppress the frequency noise by summing these two clocks (see Methods for details). We implement this differential noise suppression scheme by detecting f_{clock+} and f_{clock-} on separate photodetectors in parallel and frequency mixing the resulting heterodyne beats (Fig. 4c). In practice, we mix a frequency-divided $f_{clock+}/168$ and a copy of f_{clock-} upshifted by 40 MHz and subsequently frequency divided by 168 (Fig. 4c and Methods). The result is a noise-suppressed RF clock output at ~235 MHz.

To demonstrate OFD, we measure the frequency of the optical reference f_{871} and the RF clock output as a function of time using two synchronized counters with the two repetition rate locks in place. The results are plotted in Fig. 4d,e. The y-axis span of the optical reference is exactly 17,292 × 84 times that of the RF clock, corresponding to the OFD factor of 17,292 (equation (7)) and the electronic division factor of 84 (= 168/2) for bringing down the clock frequency to within counter and electronic mixer ranges. The LO laser is initially free-running, and we switch on the lock to the FC midway through the measurement. The RF clock frequency follows that of the LO laser, both when the laser is free-running and when it is locked. The larger frequency fluctuations in the clock trace are due to the counter measurement limitations (Methods and Supplementary Section 7).

The fractional Allan deviation of our ~235 MHz noise-suppressed RF clock output, measured using the PNTS, is plotted in Fig. 4a (green trace). The frequency instability is substantially reduced, now essentially overlaying with that of the optical reference. These results signify that the frequency stability of the 344 THz LO laser has been successfully transferred to our ~235 MHz RF clock. This suggests that our Vernier OFD system supports a fractional frequency instability of at least $\sim 3 \times 10^{-13}/\tau$. The frequency instability with longer averaging time reaches $\sim 2 \times 10^{-15}$ at 1,000 s (Fig. 4a, purple trace; see Supplementary Section 6 for more information). The performance of our OFD system is sufficient to support an atomic reference with stability better than the commercially available caesium clock with $<8.5 \times 10^{-13}$ at 100 s.

Our method also allows us to extract the differential-mode interferometric frequency noise directly (Methods), which we also plot in Fig. 4a (yellow trace).

Discussion

We have demonstrated the use of a Vernier dual-microcomb system to frequency divide an ultranarrow-linewidth 871 nm laser down to an RF output of ~235 MHz using only two feedback servos, enabled in part by an interferometric noise suppression scheme. The LO laser is tuned to within a few gigahertz of being able to be frequency doubled to a clock transition of a ytterbium ion.

The Vernier dual-microcomb OFD platform used here is useful for detecting high-frequency f_{CEO} and potentially for performing OFD on a variety of atomic species through a dual-comb sum-frequency process. Our simple dual-comb OFD architecture involving only one pump and two servo locks helps to save auxiliary photonic and electronic components, which is also of paramount importance towards ultimate development of a low size, weight and power package. With the continued advancement of microcomb system integration capabilities[38], in the future, our dual combs can potentially be integrated onto a single SiN chip, together with on-chip thermal heaters for spectral alignment and microcomb feedback, and spectral filtering for separation and routing of different wavelength bands. Furthermore, there has been exciting progress in the heterogeneous integration of III–V[39,40] and thin-film lithium niobate[41,42] materials on the SiN platform. These may enable the integration of III–V lasers for microcomb pumping and PPLN for second-order nonlinear frequency conversion towards a fully integrated dual-comb system in the future. In addition, through the elimination of many of the fibres used in our current experiment, such a system should be much less sensitive to environmental perturbations.

With further advances in compact ion traps and optical lattices[8,9,43,44], we anticipate that our dual-microcomb system, paired with an integrated atomic reference and compact narrow linewidth laser, may one day enable the development of a fully integrated high-performance optical atomic clock.

Online content

Any methods, additional references, Nature Portfolio reporting summaries, source data, extended data, supplementary information, acknowledgements, peer review information; details of author contributions and competing interests; and statements of data and code availability are available at https://doi.org/10.1038/s41566-025-01617-0.

References

1. Godun, R. M. et al. Frequency ratio of two optical clock transitions in Yb^{+171} and constraints on the time variation of fundamental constants. *Phys. Rev. Lett.* **113**, 210801 (2014).
2. Origlia, S. et al. Towards an optical clock for space: compact, high-performance optical lattice clock based on bosonic atoms. *Phys. Rev. A* **98**, 053443 (2018).
3. Riehle, F. Optical clock networks. *Nat. Photonics* **11**, 25–31 (2017).
4. Koller, S. B. et al. Transportable optical lattice clock with 7×10^{-17} uncertainty. *Phys. Rev. Lett.* **118**, 073601 (2017).
5. Hinkley, N. et al. An atomic clock with 10^{-18} instability. *Science* **341**, 1215–1218 (2013).
6. Boulder Atomic Clock Optical Network (BACON) Collaboration. Frequency ratio measurements at 18-digit accuracy using an optical clock network. *Nature* **591**, 564–569 (2021).
7. Brewer, S. M. et al. An $^{27}Al^{+}$ quantum-logic clock with a systematic uncertainty below 10^{-18}. *Phys. Rev. Lett.* **123**, 033201 (2019).
8. Ivory, M. et al. Integrated optical addressing of a trapped ytterbium ion. *Phys. Rev. X* **11**, 041033 (2021).
9. Ropp, C. et al. Integrating planar photonics for multi-beam generation and atomic clock packaging on chip. *Light Sci. Appl.* **12**, 83 (2023).
10. Papp, S. B. et al. Microresonator frequency comb optical clock. *Optica* **1**, 10–14 (2014).
11. Newman, Z. L. et al. Architecture for the photonic integration of an optical atomic clock. *Optica* **6**, 680–685 (2019).
12. Diddams, S. A., Vahala, K. & Udem, T. Optical frequency combs: coherently uniting the electromagnetic spectrum. *Science* **369**, eaay3676 (2020).
13. Diddams, S. A. et al. An optical clock based on a single trapped $^{199}Hg^{+}$ ion. *Science* **293**, 825–828 (2001).
14. Ye, J., Ma, L. S. & Hall, J. L. Molecular iodine clock. *Phys. Rev. Lett.* **87**, 270801 (2001).
15. Holzwarth, R., Zimmermann, M., Udem, T. & Hansch, T. Optical clockworks and the measurement of laser frequencies with a mode-locked frequency comb. *IEEE J. Quantum Electron.* **37**, 1493–1501 (2001).
16. Kippenberg, T. J., Gaeta, A. L., Lipson, M. & Gorodetsky, M. L. Dissipative Kerr solitons in optical microresonators. *Science* **361**, eaan8083 (2018).
17. Yu, S.-P. et al. Tuning Kerr-soliton frequency combs to atomic resonances. *Phys. Rev. Appl.* **11**, 044017 (2019).
18. Moille, G., Westly, D., Orji, N. G. & Srinivasan, K. Tailoring broadband Kerr soliton microcombs via post-fabrication tuning of the geometric dispersion. *Appl. Phys. Lett.* **119**, 121103 (2021).
19. Sun, S. et al. Integrated optical frequency division for microwave and mmWave generation. *Nature* **627**, 540–545 (2024).
20. Kudelin, I. et al. Photonic chip-based low-noise microwave oscillator. *Nature* **627**, 534–539 (2024).
21. Lai, Y.-H. et al. 871nm ultra-narrow-linewidth laser for Yb^{+} clock. In *2021 Conference on Lasers and Electro-Optics (CLEO)* (eds. Kang, J. et al.) SF2P.3 (Optica Publishing Group, 2021).

22. Lange, R. et al. Improved limits for violations of local position invariance from atomic clock comparisons. *Phys. Rev. Lett.* **126**, 011102 (2021).
23. Wu, K. et al. Vernier microcombs for high-frequency carrier envelope offset and repetition rate detection. *Optica* **10**, 626–633 (2023).
24. Yang, K. Y. et al. Bridging ultrahigh-Q devices and photonic circuits. *Nat. Photonics* **12**, 297–302 (2018).
25. Lai, Y.-H. et al. Ultra-narrow-linewidth lasers for quantum applications. In *2022 Conference on Lasers and Electro-Optics (CLEO)* STu5O.2 (Optica Publishing Group, 2022).
26. Wang, B., Yang, Z., Zhang, X. & Yi, X. Vernier frequency division with dual-microresonator solitons. *Nat. Commun.* **11**, 3975 (2020).
27. Ye, Z. et al. High-Q Si_3N_4 microresonators based on a subtractive processing for Kerr nonlinear optics. *Opt. Express* **27**, 35719–35727 (2019).
28. O'Malley, N. P. et al. Vernier frequency combs for stabilization of RF/optical links. In *2022 Conference on Lasers and Electro-Optics (CLEO)* SW4O.2 (Optica Publishing Group, 2022).
29. Stenger, J., Schnatz, H., Tamm, C. & Telle, H. R. Ultraprecise measurement of optical frequency ratios. *Phys. Rev. Lett.* **88**, 073601 (2002).
30. Del'Haye, P. et al. Phase-coherent microwave-to-optical link with a self-referenced microcomb. *Nat. Photonics* **10**, 516–520 (2016).
31. Metcalf, A. J., Torres-Company, V., Leaird, D. E. & Weiner, A. M. High-power broadly tunable electrooptic frequency comb generator. *IEEE J. Quantum Electron.* **19**, 231–236 (2013).
32. Zang, J., Briles, T. C., Morgan, J. S., Beling, A. & Papp, S. Millimeter wave frequency synthesizer based on integrated photonics. In *2020 International Topical Meeting on Microwave Photonics* 101–104 (2020).
33. Drake, T. E. et al. Terahertz-rate Kerr-microresonator optical clockwork. *Phys. Rev. X* **9**, 031023 (2019).
34. Ma, L.-S., Jungner, P., Ye, J. & Hall, J. L. Delivering the same optical frequency at two places: accurate cancellation of phase noise introduced by an optical fiber or other time-varying path. *Opt. Lett.* **19**, 1777–1779 (1994).
35. Foreman, S. M., Holman, K. W., Hudson, D. D., Jones, D. J. & Ye, J. Remote transfer of ultrastable frequency references via fiber networks. *Rev. Sci. Instrum.* **78**, 021101 (2007).
36. Newbury, N. R., Williams, P. A. & Swann, W. C. Coherent transfer of an optical carrier over 251 km. *Opt. Lett.* **32**, 3056–3058 (2007).
37. Johnson, L. A. M., Gill, P. & Margolis, H. S. Evaluating the performance of the NPL femtosecond frequency combs: agreement at the 10^{-21} level. *Metrologia* **52**, 62–71 (2015).
38. Rao, A. et al. Towards integrated photonic interposers for processing octave-spanning microresonator frequency combs. *Light Sci. Appl.* **10**, 109 (2021).
39. Xiang, C. et al. Laser soliton microcombs heterogeneously integrated on silicon. *Science* **373**, 99–103 (2021).
40. Xiang, C. et al. 3D integration enables ultralow-noise isolator-free lasers in silicon photonics. *Nature* **620**, 78–85 (2023).
41. Churaev, M. et al. A heterogeneously integrated lithium niobate-on-silicon nitride photonic platform. *Nat. Commun.* **14**, 3499 (2023).
42. Ruan, Z. et al. High-performance electro-optic modulator on silicon nitride platform with heterogeneous integration of lithium niobate. *Laser Photonics Rev.* **17**, 2200327 (2023).
43. Setzer, W. J. et al. Fluorescence detection of a trapped ion with a monolithically integrated single-photon-counting avalanche diode. *Appl. Phys. Lett.* **119**, 154002 (2021).
44. Niffenegger, R. J. et al. Integrated multi-wavelength control of an ion qubit. *Nature* **586**, 538–542 (2020).

Publisher's note Springer Nature remains neutral with regard to jurisdictional claims in published maps and institutional affiliations.

Open Access This article is licensed under a Creative Commons Attribution 4.0 International License, which permits use, sharing, adaptation, distribution and reproduction in any medium or format, as long as you give appropriate credit to the original author(s) and the source, provide a link to the Creative Commons licence, and indicate if changes were made. The images or other third party material in this article are included in the article's Creative Commons licence, unless indicated otherwise in a credit line to the material. If material is not included in the article's Creative Commons licence and your intended use is not permitted by statutory regulation or exceeds the permitted use, you will need to obtain permission directly from the copyright holder. To view a copy of this licence, visit http://creativecommons.org/licenses/by/4.0/.

© The Author(s) 2025

Methods

Experimental setup

The experimental setup is shown in Extended Data Fig. 1. We use a single-sideband modulator to rapidly frequency sweep[45] a ~1,550 nm external cavity diode laser (Toptica CTL 1550) pump into resonance for both microrings simultaneously, generating microcombs in each. The two resonators are frequency aligned using thermo-electric temperature control units. After comb generation is initiated, the pump frequency is adjusted through piezoelectric control of the external cavity diode laser towards a longer wavelength to optimize the dispersive wave conditions of the microcombs, where we obtain a high-power (~−20 dBm) short-wavelength dispersive wave emission from the main comb at ~978 nm. In this dispersive wave state, we also make use of the long-wavelength dispersive wave of the main comb, which benefits the SFG process for f-2f. A network of fibre optical filters and couplers are used to separate spectral bands at ~1,550 nm, ~2,000 nm and ~1,000 nm and combine the dual-comb spectra at ~1,550 nm and ~2,000 nm. For the results shown in the main text, we have introduced foam partitions to cover most of our setup to reduce noise effects due to air currents and the like (for further discussion, see Supplementary Section 3).

The combined 2,000 nm spectral components are amplified using a thulium-doped fibre amplifier and then distributed in three arms for (1) the SFG process for f-2f, (2) the SFG process to hit 871 nm via combining with the 1,550 nm residual pump from the Vernier comb and (3) the Vernier beat detection. The SFG products for f-2f are subsequently amplified by a semiconductor optical amplifier (Innolume) and filtered by a 1-nm-bandwidth bandpass filter (Photonwares) to suppress the broadband amplified spontaneous emission noise. It is then combined with the ~1,000 nm light from the main comb to generate the f-2f beat $f_{\text{f-2f}}$ using a balanced photodetector (BPD). The SFG products at 871 nm from the Vernier comb are combined with 25% of the 871 nm LO laser using a 75:25 coupler to generate $f_{\text{comb-LO}}$, with ~−36 dBm of SFG (spectrum shown in Fig. 2d) and ~−4.5 dBm of laser power measured at the photodetector. Seventy-five per cent of the LO laser is combined with the FC (bandpass-filtered at ~871 nm) using a 50:50 coupler and $f_{\text{LO-FC}}$ is detected on another BPD, with ~3 dBm of LO power and ~−56 dBm power per FC line at one arm of the BPD (where the laser and FC spectra in Fig. 2d are measured). The clocks at both sides of the pump are selected by a programmable optical filter (Finisar), optically amplified in the same erbium-doped fibre amplifier and separated by a dense wavelength-division multiplexing filter for detection on two distinct photodetectors.

The Vernier beat f_{Vernier} detected by an amplified photodetector is divided by 8 and sent to an offset phase lock servo (Vescent D2-135). We obtain $f_{\text{xCEO}}/8$ by mixing $f_{\text{f-2f}}$ divided by 8 and $f_{\text{comb-LO}}$ divided by 16. This beat is sent to another phase lock servo. We use two stable RF synthesizers (Agilent E8257D and Keysight 33600A) as the frequency references for $f_{\text{Vernier}}/8$ and $f_{\text{xCEO}}/8$, synchronized to a 10 MHz GPSDO (EndRun Meridian). Finally, for our frequency instability measurements, we use frequency counters (Keysight 53230A) and a PNTS (Microsemi 5125A), which will be discussed in the Noise-suppressed RF clock section.

Interferometric noise suppression scheme

In Fig. 4b, we show the phase fluctuations in the upper and lower arms as $\phi_1(t)$ and $\phi_2(t)$, respectively. $\phi_1(t)$ is composed of the time-varying phase experienced by the pump in the interferometer arm upstream of the main ring plus the phase picked up by the comb line of interest downstream from the main ring; $\phi_2(t)$ is defined similarly but refers to the leads connecting the Vernier ring. As illustrated in Fig. 4c, we term the two clocks detected at different sides of the pump $f_{\text{clock+}}$ and $f_{\text{clock−}}$, corresponding to the higher- and lower-frequency side, respectively,

$$f_{\text{clock+}} = \left[f_{\text{pump}} + f_{\text{rep1}} + \frac{\phi_1'(t)}{2\pi}\right] - \left[f_{\text{pump}} + f_{\text{rep2}} + \frac{\phi_2'(t)}{2\pi}\right], \tag{8}$$

$$f_{\text{clock-}} = \left[f_{\text{pump}} - f_{\text{rep2}} + \frac{\phi_2'(t)}{2\pi}\right] - \left[f_{\text{pump}} - f_{\text{rep1}} + \frac{\phi_1'(t)}{2\pi}\right], \tag{9}$$

where $\phi'(t)$ represents the time derivative of $\phi(t)$. These expressions take into account the frequency fluctuations that arise in proportion to the derivative of the time-varying phases[46]. Because $\phi_1(t)$ and $\phi_2(t)$ may be uncorrelated, they give rise to frequency noise on the clock signal. Critically, the frequency noise on $f_{\text{clock+}}$ and $f_{\text{clock−}}$ is equal and opposite in the expressions above. By summing $f_{\text{clock+}}$ and $f_{\text{clock−}}$ with an electronic mixer

$$f_{\text{clock+}} + f_{\text{clock-}} = 2(f_{\text{rep1}} - f_{\text{rep2}}), \tag{10}$$

we can ideally suppress the frequency noise completely. Note that the formulation above ignores any noise contributed by the electronics and approximates the phase shifts incurred by comb lines ±1 in the fibre leads downstream of the resonators as equal. Because the frequencies of the ±1 modes differ from the pump frequency by only a small fractional amount, the error involved in this approximation is small. Further analysis on the noise suppression scheme can be found in Supplementary Section 4.

Noise-suppressed RF clock

Our noise suppression scheme relies on mixing $f_{\text{clock+}}$ and $f_{\text{clock−}}$ to cancel differential-mode noise in the RF clock output. We mix frequency-divided versions of these two signals in practice ($f_{\text{clock+}}/168$ and $f_{\text{clock−}}/168$). Importantly, the sum of these two signals is almost exactly equal to the second harmonic of either (that is, $f_{\text{clock+}}/168 + f_{\text{clock−}}/168 \approx 2f_{\text{clock+}}/168 \approx 2f_{\text{clock−}}/168$). This means that it is impossible to filter out the undesirable second harmonics originating in the mixer and get the pure sum-frequency signal, thus still resulting in excess noise. To avoid this problem, we frequency shift one of the clocks by mixing with the 40 MHz signal (generated by twice-doubling the 10 MHz GPS-disciplined reference) to obtain $f_{\text{clock−}}$ + 40 MHz, filtered by a 30-MHz-bandwidth yttrium iron garnet bandpass filter. This frequency-upshifted clock is being divided and electronically mixed with the other divided clock to realize $f_{\text{clock+}}/168 + (f_{\text{clock−}} + 40\ \text{MHz})/168$ at the output. The desired sum-frequency output is then distinguishable from harmonics of either of the mixer inputs. Although the second harmonic and other products still exist and are spaced by ~238 kHz (40 MHz/168), the desired noise-suppressed output is ~20 dB higher than the other products and the PNTS can track the desired signal (see Supplementary Fig. 8 for the RF spectrum). Importantly, we note that the 10 MHz reference used here to shift one of the clock products should in principle be able to be derived from an optical reference if our system were to perform OFD on an atomic specimen (somewhat similar to ref. 13). This would remove the need for a GPS-referenced 10 MHz sync signal to operate the OFD system.

For Fig. 4d,e, we measure the frequency traces of the optical reference and the RF clock output simultaneously on two synchronized frequency counters running at 100 ms gate time with the same trigger signal and external gate. The optical reference frequency f_{871} is obtained by recording $f_{\text{LO-FC}}$ and calculating f_{871} using equation (6). We attribute the larger frequency fluctuations in the RF clock trace compared with the optical reference to the spurious frequency content in the output signal in addition to the typical counter timing jitter-related resolution limit. Although the weak spurs cause no notable problem for the PNTS (because the noise-equivalent bandwidth of PNTS at 1 ms gate time is 500 Hz and spurs fall outside the band), they do result in a few-fold increase in the frequency fluctuations reported by the frequency counter (see Supplementary Sections 7 and 8 for further discussion).

The Allan deviation for the RF clock output and the FC (Menlo Systems) reference were taken several times over multiple days. The symbols and error bars plotted in Fig. 4a represent the averages and standard deviations from multiple measurement results. The error bars are relatively tight, indicating good repeatability.

Interferometric noise extraction

The noise suppression scheme can be modified to extract the interferometric noise for direct measurement. As explained in the main text, by adding f_{clock+} and f_{clock-} the differential frequency noise can be made to cancel out. By measuring the difference between f_{clock+} and f_{clock-}, the clock term is cancelled and we obtain the frequency noise term $\delta f_N(t)$. To implement the noise measurement, we frequency upshift one of the clocks by 200 MHz and divide it by 168, then frequency mix with the other clock also divided by 168 (Extended Data Fig. 2). This creates a frequency difference of ~1.2 MHz out of the mixer, which is within the frequency range of our PNTS (1–400 MHz). The fractional instability of this signal filtered using a low-pass filter (normalized to the ~235 MHz noise-suppressed clock frequency) is shown as the yellow curve in Fig. 4a and is similar to the curve for the clock output without noise suppression.

Data availability

The data used to produce the plots within this Article are available via Figshare at https://doi.org/10.6084/m9.figshare.23971425 (ref. 47).

Code availability

The code used to produce the plots within this Article is available via Figshare at https://doi.org/10.6084/m9.figshare.23971425 (ref. 47).

References

45. Stone, J. R. et al. Thermal and nonlinear dissipative-soliton dynamics in Kerr-microresonator frequency combs. *Phys. Rev. Lett.* **121**, 063902 (2018).
46. Weiner, A. M. *Ultrafast Optics* (Wiley, 2011).
47. Wu, K., O'Malley, N. P., Fatema, S. & Weiner, A. M. raw data for 'Vernier microcombs for integrated optical atomic clocks'. *Figshare* https://doi.org/10.6084/m9.figshare.23971425 (2024).

Acknowledgements

This work was funded in part by the Defense Advanced Research Projects Agency APhI programme (to A.M.W. and M.Q.), by the Air Force Office of Scientific Research under grant FA9550-20-1-0283 (to A.M.W.) and by the Swedish Research Council (grant nos. 2020-00453 and 2022-06575 to V.T.-C.). M.S.A. acknowledges support from the Researchers Supporting Project number (RSPD2025R613), King Saud University, Riyadh, Saudi Arabia. M.Q. also acknowledges support from the U.S. National Science Foundation under grant DMR-2323752. The effort at Purdue under the Defense Advanced Research Projects Agency APhI programme was part of a project team lead by Sandia National Laboratories. The Si_3N_4 fabrication was done at Myfab Chalmers. We thank S. Diddams, S. Papp, F. Quinlan, X. Yi and B. Wang for fruitful discussion. J. Zang suggested the experiment shown in Supplementary Fig. S3 for the diagnosis of the phase noise issue. M. Kickbush and M. Abu Khater assisted in identifying appropriate yttrium iron garnet filters for our system. H. McGuinness kindly reviewed the manuscript before submission. We are indebted to the late A. M. Weiner for his invaluable guidance and wisdom in shaping this work. His dedicated involvement and insightful contributions to various aspects of this project were crucial. Some of our earlier work on Vernier dual combs, such as dual-octave comb pairs, was presented at the Conference on Lasers and Electro-Optics (CLEO) 2021 (SW2H.7), CLEO 2022 (SW4O.2) and CLEO 2023 (STh1J.4 and STh1J.5).

Author contributions

A.M.W., M.S.A. and M.Q. devised the Vernier dual-comb scheme and initiated the project. K.W., N.P.O. and S.F. devised and conducted the experiments. C.W. designed the microring devices. M.G. and Z.Y. were responsible for fabrication of the microring devices, with oversight from V.T.-C. D.E.L. was responsible for putting in place laboratory systems and advised on some of the experiments. A.M.W. supervised the project. K.W., N.P.O., S.F. and A.M.W. wrote the manuscript.

Competing interests

The authors declare no conflicts of interest.

Additional information

Extended data is available for this paper at https://doi.org/10.1038/s41566-025-01617-0.

Supplementary information The online version contains supplementary material available at https://doi.org/10.1038/s41566-025-01617-0.

Correspondence and requests for materials should be addressed to Kaiyi Wu.

Peer review information *Nature Photonics* thanks Nils Nemitz and the other, anonymous, reviewer(s) for their contribution to the peer review of this work.

Reprints and permissions information is available at www.nature.com/reprints.

https://doi.org/10.1038/s41566-025-01617-0

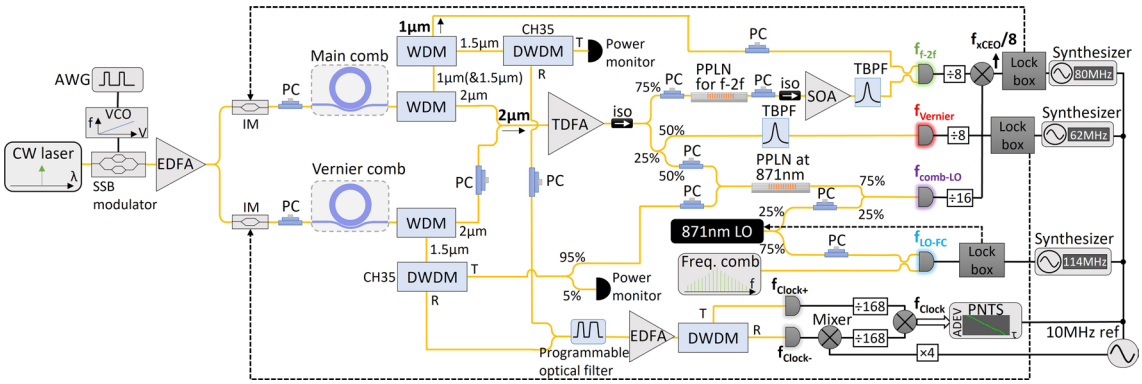

Extended Data Fig. 1 | Experimental setup. CW: continuous wave. AWG: arbitrary waveform generator. VCO: voltage-controlled oscillator. SSB modulator: single sideband modulator. EDFA: erbium-doped fiber amplifier. IM: intensity modulator. TDFA: thulium-doped fiber amplifier. PC: polarization controller. WDM: wavelength-division multiplexing. DWDM: dense wavelength-division multiplexing. iso: isolator. SOA: semiconductor optical amplifier. BPF: bandpass filter. TBPF: tunable bandpass filter. PNTS: phase noise test set.

https://doi.org/10.1038/s41566-025-01617-0

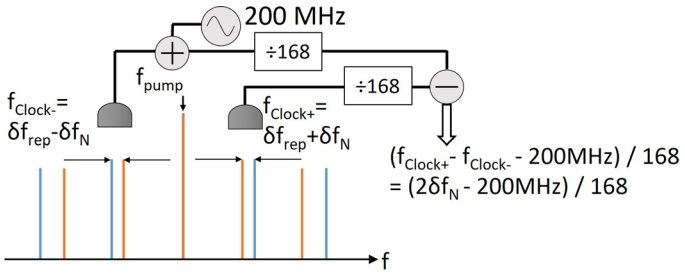

Extended Data Fig. 2 | Interferometric noise extraction. Illustration of the experimental configuration.